Magnetic Resonance Imaging 61 (2019) 296–299

Contents lists available at ScienceDirect

Magnetic Resonance Imaging

journal homepage: www.elsevier.com/locate/mri

Case report

Phase enhanced PSIR T1 weighted imaging improves contrast resolution of the nucleus basalis of Meynert at 7 T: a preliminary study

Ketan Jethwa[a,b,*], Kingkarn Aphiwatthanasumet[a], Olivier Mougin[a], Richard Bowtell[a], Dorothee Auer[a,b], Penny Gowland[a]

[a] National Institute of Health Research Nottingham Biomedical Research Centre, Queens Medical Centre, Derby Road, Nottingham NG7 2UH, United Kingdom
[b] Sir Peter Mansfield Imaging Centre, University Park, University of Nottingham, NG7 2RD, United Kingdom

ARTICLE INFO

Keywords:
Magnetic resonance imaging
Nucleus basalis of Meynert
Phase sensitive inversion recovery
Susceptibility weighted imaging

ABSTRACT

Background: The nucleus basalis of Meynert (NBM) provides the majority of cortical cholinergic innervation which is required for memory formation, maintaining attention and promoting learning. Neuronal loss within this area is implicated in a number of neurodegenerative disorders. Imaging the NBM is however limited by its small size and suboptimal contrast resolution at the base of the brain.
Purpose: To develop a novel method of processing T1 weighted MRI data for improving contrast resolution and delineation of the NBM.
Study type: Technical development, case series.
Subjects: Five healthy volunteers.
Field strength, sequence, analysis: Volunteers were scanned on a Philips 7 T Achieva imaging system. T1-weighted images were constructed from a double inversion phase sensitive inversion recovery (PSIR) sequence. Inversion recovery data were combined with the filtered phase data from the long inversion time image to produce a novel susceptibility weighted-PSIR (SW-PSIR) map. This process is similar to that used to combine T2* weighted image and phase maps to create susceptibility weighted images (SWI), but with the processing parameters optimized in terms of contrast-to-noise ratio to the NBM in the final SW-PSIR maps. Average NBM thickness was reported as mean ± standard deviation (SD). Intra-observer and inter-observer reliability were tested using intra-class correlation coefficient (ICC).
Results: 0.7mm^3 isotropic resolution images were acquired in a 5 min and 50 s scan. The mean thickness ± SD of the left (right) NBM was 3.5 ± 0.4 mm and 3.8 ± 0.5 mm (3.6 ± 0.5 mm and 3.7 ± 0.5 mm) by the first and second observers respectively with excellent intra-observer and inter-observer agreement (> 0.90).
Conclusion: In this pilot study the SW-PSIR imaging approach improves delineation of the NBM between the ventral pallidum and chiasmatic cistern allowing accurate thickness measurement. The role of this sequence, in enabling robust morphometry of the NBM in health and disease, can be tested further in larger studies.

1. Introduction

The subcommissural basal forebrain is a region located above the chiasmatic cistern and inferior to the ventral pallidum and decussation of the anterior commissure. This brain area is of strategic importance as it contains a population of hyperchromic magnocellular neurones which provide the majority of cholinergic innervation to the neocortex [1]. The greatest concentration of cholinergic neurones are found anteriorly in the subcommissural and subpallidal regions within an area termed the 'nucleus basalis of Meynert' (NBM). The NBM is of importance in health and disease as it is the primary source of cortical acetylcholine, a neurotransmitter required for associative learning, memory formation and attention. Cholinergic deficits, due to neuronal cell loss in the NBM or pharmacological cholinergic blockade, produce memory and attentional deficits in humans. The NBM is affected early in the course of a number of neurodegenerative disorders, including Alzheimer's disease, where the deposition of pathological proteins (hyperphosphorylated tau) leads to cell loss, reduced cerebral cholinergic concentrations and clinical cognitive impairments [1]. However, the NBM is difficult to image due to its small size, proximity to a brain-cerebrospinal fluid interface and borderline contrast resolution at the base of the brain. The development of a novel imaging sequence for

* Corresponding author at: Radiological Sciences, University of Nottingham, Queens Medical Centre, Derby Road, Nottingham NG7 2UH, United Kingdom.
E-mail address: ketan.jethwa@nottingham.ac.uk (K. Jethwa).

https://doi.org/10.1016/j.mri.2019.06.004
Received 26 March 2019; Received in revised form 29 May 2019; Accepted 2 June 2019

improved NBM delineation will therefore help researchers and clinicians to better assess NBM changes in vivo and correlate these with cognitive measures. The purpose of this study was to develop a high resolution, high contrast acquisition and analysis protocol for in vivo imaging of the NBM using high field (7 T) MRI. We hypothesized that the grey/white matter contrast could be enhanced through phase mask filtering of inversion recovery images at ultrahigh field for improved visualization of the NBM in vivo. We tested this hypothesis in young healthy volunteers in this proof-of-concept pilot study.

2. Methods and materials

Data were collected following Sir Peter Mansfield (University of Nottingham) ethical review board approval. Written informed consent was obtained from all participants in the study.

2.1. Participants

Five healthy volunteers (mean age 29 years) were scanned on a Philips 7 T Achieva system with T/R 1/32 channel head coil (Nova Medical, Wilmington, MA). Contrast media was not administered.

2.1.1. Data acquisition

3D T1-weighted phase sensitive inversion recovery (PSIR) imaging was acquired as previously described in [2] using an inversion pulse tailored to overcome B1 errors [3]. Dielectric pads ($18 \times 18 \times 0.8\,cm^3$, containing a suspension of calcium titanate with weights in ratio 2.8:1 in deuterated water [4–6]) were placed over the subject's ears to produce a more homogeneous B1 field. No parallel imaging was used to maximize sensitivity at the centre of the field of view. This allowed a relatively narrow right-left (RL) field of view to be used with RL phase encoding to speed up imaging. The protocols used for the repeatability study were: TR = 6.3 ms, TE = 2.8 ms, flip angle of 5°, field of view (AP, RL, FH) = $70 \times 191 \times 180$ mm, isotropic resolution of $0.7\,mm^3$ with a total acquisition time of 5 min 50 s. T1 weighted images were acquired using the dual readout Phase-Sensitive Inversion Recovery (PSIR) sequence with TI_1 = 780 ms, TI_2 = 2380 ms, and acquisition of 100 gradient echoes per shot. These timings had previously been optimized for grey/white matter contrast across the whole brain [2]. This sequence uses the same source data as the MP2RAGE sequence. The T1 weighted PSIR image is reconstructed using

$$PSIR = \frac{\pm|SI_1|}{|SI_1| + |SI_2|} \quad (1)$$

where signal SI_1 is the short inversion time (TI_1) and signal SI_2 is the long inversion time (TI_2). PSIR imaging demonstrates improved contrast-to-noise ratio compared to MP2RAGE and there is minimal difference in absolute tissue contrast between the two methods of reconstruction [2]. Typical images are shown in Fig. 1.

2.1.2. Data processing

The magnitude and phase images were combined to produce susceptibility weighted PSIR images (SW-PSIR) by adapting the method previously proposed for susceptibility weighted imaging [8]:

$$\text{SW-PSIR}_i = S_i(f_i)^n \quad \text{for} \quad i = 1...M \quad (2)$$

where

$$f_i = \frac{[\pi + \varphi_i]}{\pi} \text{for} -\pi < \varphi_i < 0 \quad (3)$$

$$f_i = 1 \text{ for } \varphi_i > 0 \quad (4)$$

$\text{SW} - \text{PSIR}_i$ is the signal in the i^{th} voxel of the final image and S_i is the signal in the i^{th} voxel of the PSIR image (Eq. (1)). φ_i is the signal in the i^{th} voxel of the filtered phase map for the long inversion time (TI_2) image; this phase map was used since there was no phase inversion from the inversion pulse in this late inversion time image. A homodyne filter of width 10 pixels was used to obtain high-pass filtered phase images. Then, a normalized phase mask was calculated using Eqs. (3) and (4) under the assumption that the phase of interest is negative. Finally, the normalized phase mask was combined with the original PSIR image according to Eq. (2) to create a susceptibility weighted PSIR image (SW-PSIR). The value of n was varied from 3 to 6 to optimize the processing of these short TE, T1 weighted inversion recovery images (n = 4 is used in standard SWI reconstruction [8]). All data processing was performed in MATLAB (The MathWorks, Natick, Massachusetts, USA, R2012a).

2.1.3. Image analysis

FSL's Brain Extraction Tool (BET) was used to extract brain tissue for image analysis [9]. A coronal section was used to determine the boundaries of the NBM, starting at the first slice where hemispheric crossing of the anterior commissure was observed. An open source image analysis program, ImageJ [10], was used to draw region of interest (ROIs) and distances for the following quantitative measurements.

The CNR was assessed between the NBM and surrounding tissue:

$$CNR = \frac{|Tissue_1 - Tissue_2|}{Noise} \quad (5)$$

where $Tissue_1$ and $Tissue_2$ are the mean signal intensity in the NBM (red ROI in Fig. 2) and midline anterior commissure (purple ROI in Fig. 2). *Noise* was estimated as the standard deviation in a homogeneous region of white matter (green) as the data was acquired with standard background filtering. The contrast was compared between the standard PSIR image and SW-PSIR images with different values of n to optimize the choice of n and compare the new SW-PSIR images to standard PSIR images. This comparison was performed as SW was added to PSIR imaging. In addition, PSIR imaging has previously been shown to have

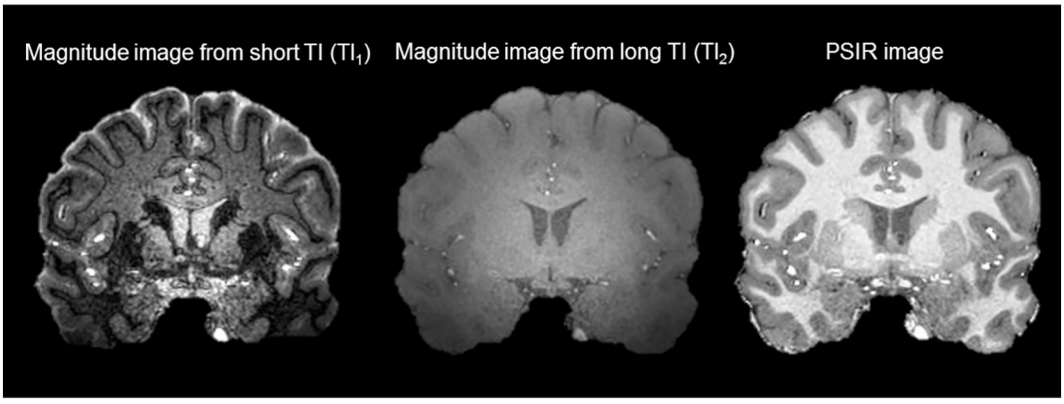

Fig. 1. Coronal magnitude images from short inversion time TI_1 (left), long inversion timeTI_2 (middle) and the resulting PSIR image through the NBM in vivo (right).

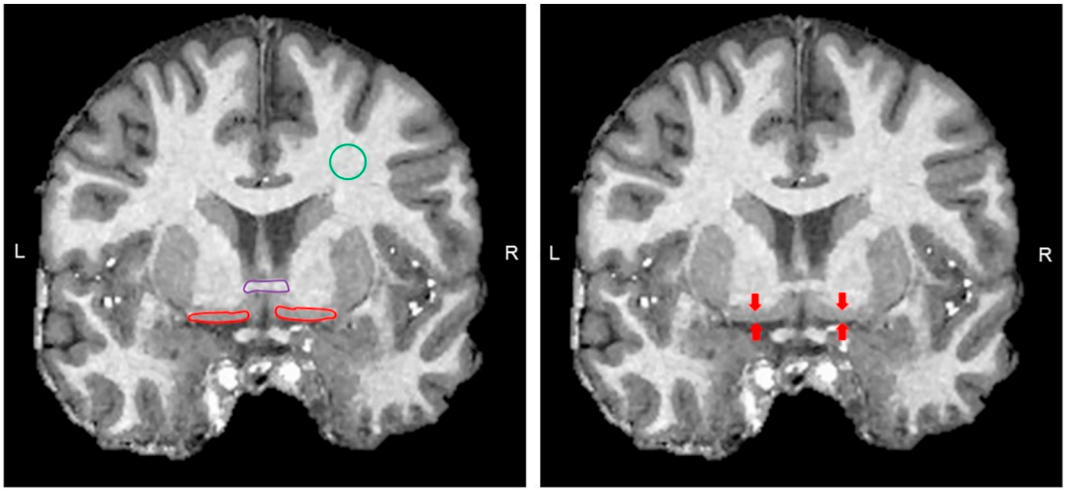

Fig. 2. Definition of ROIs on PSIR image to evaluate CNR in the NBM on a coronal slice in an anterior segment. Manual ROIs were drawn in the NBM (red), crossing fibres of the anterior commissure (purple) and a region in white matter (green). Red arrows indicate where the NBM thickness was measured. (For interpretation of the references to color in this figure legend, the reader is referred to the web version of this article.)

superior CNR and similar visible tissue contrast to MP2RAGE imaging [2].

The thickness of the NBM was measured, at its midpoint, on a single coronal image with the anterior commissure in the midline on the SW-PSIR data (vertical line from inferior most aspect of the ventral pallidum to the base of the brain (Fig. 2)) by two observers making five repeated measurements for each subject. Observer 1 was a radiographer (KK) and observer 2 was a radiologist (KJ) and each was blinded to each other's results. Thickness measurements for the two raters are presented below, in Table 1. Intra-class correlation coefficient (ICC) and 95% confidence intervals were calculated for both intra-observer and inter-observer reliability, classified as minimal (ICC ≤ 0.25), low (0.26 ≤ ICC ≤ 0.50), moderate (0.50 ≤ ICC ≤ 0.70), high (0.70 ≤ ICC ≤ 0.90), or excellent (ICC ≥ 0.90).

3. Results

The NBM was well delineated and localised on the 7 T T1 weighted SW-PSIR image (Figs. 2 and 3).

The intra-observer and inter-observer ICC values (95% CI) are shown in Table 2. The ICC values for NBM thickness have excellent intra-observer and inter-observer agreement.

4. Discussion

In this study, we have developed a susceptibility and T1 weighted scan for imaging the NBM at 7 T MRI with high spatial resolution (0.7 mm^3 isotropic resolution) in a reasonable imaging time (5 min 50 s) (SW-PSIR- multiplying the PSIR scan by the phase raised to the power of 5).

We showed that combining filtered phase and magnitude data in the SW- PSIR images improved the CNR between the NBM and the ventral pallidum (grey matter structures) compared to standard PSIR. Improved contrast resolution of the NBM allowed accurate NBM thickness measurements which are repeatable between assessors. The good interrater reliability, demonstrated in this preliminary study, is encouraging for future applications where measurements between assessors or subjects (at different time points) are compared.

This processing was specifically optimized for the NBM, and could reduce the contrast at the grey/white matter or grey matter/CSF border, but since the SW-PSIR images are produced with no cost to scan time, both the original PSIR images and SW-PSIR images can be made available for segmentation if required. This SW-PSIR approach could also be adapted for use in other areas of the brain, reoptimizing the scaling of the phase mask in the SWI calculation (n) for different datasets.

However, the optimum value of n was found to be larger here than used in T2* weighted SWI images, probably due to the shorter TE required for the T1 weighted PSIR scan. Imaging at the base of the brain is susceptible to subtle motion and artefacts from the large intracranial vessels particularly in SWI enhanced sequences. However, the SWI-PSIR sequence is less susceptible to these artefacts because of the use of a short TE and sufficient phase sensitivity at 7 T.

The lack of parallel imaging, used to maximize SNR at the centre of the brain, will have the additional benefit of making the protocol robust in patient populations. The PSIR sequence uses an inversion pulse and two turbo field echo (TFE) readouts and both of these components of the sequence can be sensitive to B1 inhomogeneity particularly in this area of the brain. Therefore, a tailored inversion pulse with low sensitivity to RF variation [7] and dielectric pads [8–10] were used to reduce these effects. In future it would be useful to acquire a B1 map in all cases to determine the effect of variation in B1 on the final results and possibly modify the sequence flip angles at time of data acquisition to limit the consequences of variation in RF amplitude [7,11].

The purpose of this proof-of-concept pilot study was to determine whether a SW-PSIR could increase NBM contrast resolution. Within this small cohort we have shown that the delineation of the anatomical boundaries of the NBM is improved with this sequence and can be used to quantify NBM thickness. The role of this new sequence in assessing NBM morphometry in health and disease requires testing in larger populations.

Table 1
shows the average thickness of the NBM in young healthy volunteers (n = 5). There were no statistically significant differences between left and right NBM for all volunteers considered (p > 0.05).

Subject	Age	Sex	Average NBM thickness (mm)			
			Observer 1		Observer 2	
			L	R	L	R
1	32	F	3.43	3.60	3.58	3.52
2	29	M	4.23	4.41	4.70	4.23
3	25	M	3.03	3.00	3.33	2.99
4	25	M	3.43	3.50	3.66	3.60
5	35	M	3.48	3.69	3.82	3.96
Mean ± SD	29.2		3.5 ± 0.4	3.6 ± 0.5	3.8 ± 0.5	3.7 ± 0.5

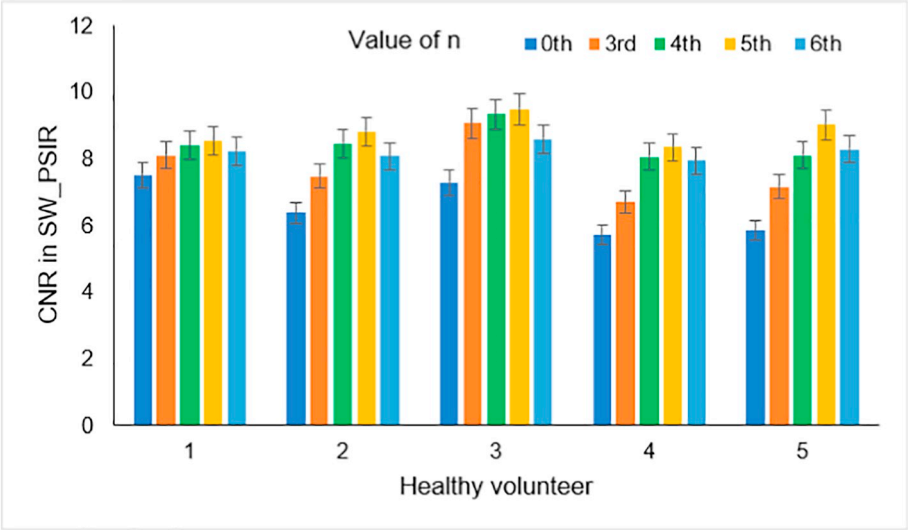

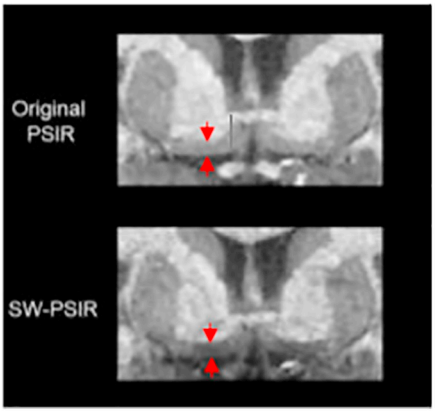

Fig. 3. CNR in SW- PSIR (averaged over both left and right NBM) for phase data raised to power of n = 3, 4, 5 and 6 (Eq. (3)) compared with original PSIR (n = 0). Representative images for volunteer 1 for the standard PSIR scan and for SW-PSIR with n = 5. There is improved boundary delineation of the NBM between the NBM, ventral pallidum/anterior commissure and chiasmatic cistern with SW-PSIR compared to the PSIR image.

Table 2
Intra-class correlation coefficient (ICC) showing inter and intra-observer reliability for measurements of NBM thickness.

Side of brain	Inter-observer ICC	Intra-observer ICC	
		Observer 1	Observer 2
Measurements of NBM thickness			
L	0.984 (0.848–0.998)	0.898 (0.621–0.998)	0.919 (0.700–0.991)
R	0.968 (0.690–0.997)	0.915 (0.683–0.990)	0.914 (0.679–0.990)

Note: 95% confident interval (lower bound-upper bound).

Improving the contrast resolution at the base of the brain will help facilitate accurate morphometry of the basal forebrain cholinergic nuclei and future clinical applications may include morphological assessments of the NBM across the aging-dementia spectrum.

In this preliminary study we have developed a 7 T PSIR scanning protocol and new method of processing the imaging data to produce high contrast and spatial resolution SW-PSIR images of the NBM.

References

[1] Mesulam MM. Cholinergic circuitry of the human nucleus basalis and its fate in Alzheimer's disease. J Comp Neurol 2013;521(18):4124–44.
[2] Mougin O, Abdel-Fahim R, Dineen R, Pitiot A, Evangelou N, Gowland P. Imaging gray matter with concomitant null point imaging from the phase sensitive inversion recovery sequence. Magn Reson Med 2016;76(5):1512–6.
[3] Hurley AC, et al. Tailored RF pulse for magnetization inversion at ultrahigh field. Magn Reson Med 2010;63(1):51–8. https://doi.org/10.1002/mrm.22167.
[4] Brink WM, van der Jagt AMA, Versluis MJ, Verbist BM, Webb AG. High permittivity dielectric pads improve high spatial resolution magnetic resonance imaging of the inner ear at 7 T. Invest Radiol 2014;49(5):271–7.
[5] Teeuwisse WM, Brink WM, Webb AG. Quantitative assessment of the effects of high-permittivity pads in 7 Tesla MRI of the brain. Magn Reson Med 2012;67(5):1285–93.
[6] Teeuwisse WM, Brink WM, Haines KN, Webb AG. Simulations of high permittivity materials for 7 T neuroimaging and evaluation of a new barium titanate-based dielectric. Magn Reson Med 2012;67(4):912–8.
[7] Jenkinson M, Beckmann CF, Behrens TEJ, Woolrich MW, Smith SM. FSL. Neuroimage 2012;62(2):782–90.
[8] Haacke EM, Xu Y, Cheng Y-CN, Reichenbach JR. Susceptibility weighted imaging (SWI). Magn Reson Med 2004;52(3):612–8.
[9] Smith SM. BET: brain extraction tool. Rev Lit Arts Am 2006;39(1):25.
[10] Schneider CA, Rasband WS, Eliceiri KW. NIH image to ImageJ: 25 years of image analysis. Nat Methods 2012;9(7):671–5.
[11] Nehrke K, Börnert P. DREAM - a novel approach for robust, ultra-fast, multi-slice. Imaging 2012;68(5):1517–26. https://doi.org/10.1002/mrm.24158. Epub 2012 Jan 17.